ISSN 0031-918X, The Physics of Metals and Metallography, 2015, Vol. 116, No. 10, pp. 1035–1046. © Pleiades Publishing, Ltd., 2015.

STRENGTH AND PLASTICITY

Effect of Friction Stir Processing on the Microstructure and Hardness of an Aluminum–Zinc–Magnesium–Copper Alloy with Nickel Additives[1]

Haider T. Naeem, Kahtan S. Mohammed, and Khairel R. Ahmad

School of Materials Engineering, University Malaysia Perils, 02600 Jejawi, Perlis, Malaysia

e-mail: haider neem@yahoo.com

Received June 9, 2014; in final form, January 20, 2015

Abstract—The main object of this study is to investigate the effect of friction stir processing (FSP) on the microstructure and hardness of Al–Zn–Mg–Cu alloys that were produced via casting with the addition of 5 wt % nickel. Furthermore, a single-pass FSP with a rotational speed of 1500 rpm and a traveling speed of 40 mm/min was performed on the alloys. The FSP-treated cast alloys were homogenized, aged at 120°C for 24 h, retrogressed at 180°C for 30 min, and then re-aged at 120°C for 24 h. Microstructural evaluations via optical microscopy and scanning electron microscopy, as well as with energy dispersive X-ray spectroscopy were conducted. In addition, X-ray diffraction analysis was performed to detect the intermetallics and phases of the Al–Zn–Mg–Cu–Ni alloys. Before FSP, the microstructural observations indicated the presence of coarse Ni dispersed particles with a precipitate phase within the matrix. After FSP treatment, the grain refinement led to the uniform space distribution of Ni dispersed particles in the stir zone. The Vickers hardness values for the Al–Zn–Mg–Cu–Ni alloy increased after age tempering at T6 and retrogression and re-aging (RRA) treatment because of the increased precipitation and particles dispersity. The hardness of the Al–Zn–Mg–Cu–Ni alloy was enhanced after FSP and a series of heat treatments, especially the RRA process, because of the stirring action of the FSP tool, the grain refinement, the appearance of additional precipitates, and the refinement of dispersed Ni particles.

Keywords: friction stir processing, aluminum alloy, nickel additives, grain refinement

DOI: 10.1134/S0031918X15100051

1. INTRODUCTION

A 7000 Al alloy series has high strength, high elongation, high wear resistance, high temperature performance, and low density. This alloy never failed to capture the fascination of metallurgical and material scientists and is widely used in the aviation and aerospace industries. To date, the highest reported tensile strength of the Al alloy is about 445 MPa to 500MPa [1]. The shear elastic modulus of the Al alloy is about 26 GPa, and its maximum strength can theoretically reach up to 870 MPa. The properties of the the Al alloy can still be significantly improved. To strengthen the Al alloy, several conventional and unconventional processing techniques have been developed. The first category of these techniques include precipitation [2], dispersion strengthening [3], and chemical modification, which are achieved by adding a small amount of transition metals, such as Zr [4], Ti [5], and Ni, [6] into the Al alloy, thereby enhancing the microstructure of the matrix. The second categories of these techniques include equal channel angular extrusion [7], accumulative roll bonding [8], and friction stir processing (FSP) [9]. FSP is a novel solid-state process of modifying the microstructure of the cast and produced Al alloys. In FSP, a rotating tool with a pin and shoulder is inserted into a piece of material and traverses along the work piece. The thermal exposure and intense plastic deformation of the material would result in a significant evolution of the local microstructure. The details of the FSP principles are found elsewhere [10, 11]. In the present study, Ni was added into an Al–Zn–Mg–Cu alloy via a semi-chilled casting process followed by the application of FSP, which significantly disrupts the coarse Ni particles and generates a homogeneous distribution of Al–Ni intermetallic compounds. In addition, the effect of heat treatment applied during FSP and its influence on the mechanical properties of the Al alloy were investigated. Studies have indicated that FSP results in a substantial grain refinement of the Al–Zn–Mg–Cu alloy, thereby leading to the improvement of its mechanical properties [12, 13].

Rayes et al. [14] have concluded that FSP enhances the ductility and mechanical properties of the 7010 Al alloy at high temperatures. Hu et al. [15] conducted a study to refine the grain size of the Al–Zn alloy via FSP. To date, no studies have been reported on the

[1] The article is published in the original.

Table 1. Chemical compositions of the Al alloy (wt %)

No.	Si	Fe	Cu	Mg	Cr	Ni	Zn	Ti	Al
Alloy	0.10	0.20	1.70	2.80	0.186	5.00	7.01	0.047	Balance

Table 2. Heat treatment steps for alloys being studied

No.	Type	Details of treatment
1	Homogenizing	450°C for 2 h + 470°C for 24 h + 480°C for 0.5 h
2	Aging (T6)	120°C for 24 h (peak ageing)
3	Retrogression & Reaging (RRA)	120°C for 24 h +180°C for 0.5 h (retrogression) + 120°C for 24 (re-aging)

addition of Ni into the 7000 Al alloy series treated via FSP. This study compares the microstructure and hardness of Al–Zn–Mg–Cu alloys with Ni before and after application of FSP at different heat treatment conditions.

2. EXPERIMENTAL PROCEDURES

To prepare the experimental alloy, the AA7075-O Al alloy ingot was re-melted in a graphite crucible at 830°C by using an electrical resistance furnace. Afterward, 5 wt % Ni (particle size (μm) about D50 of 11, rounded shape, purity (%) of 99.50: source Merck KGaA) was then added. Table 1 presents the nominal composition of the Al alloy being studied.

The alloys were produced via a semi-direct chill (DC) casting process. The alloys were poured into a pre-heated (250°C) rectangular mold with dimensions of 160 mm × 22 mm × 17 mm at 830°C. The alloys were inverted and re-melted three times to ensure complete mixing. The first group of the Al alloy was denoted as alloy A (as cast), and the second group was denoted as alloy B (as plates). After machining, the alloys were processed via single-passed FSP by using a HD CNC milling machine. A stainless steel tool with a flat shoulder and threaded tapered pin was used, as is shown in Fig. 1 along with its dimensions. In all experiments, the tool angle was fixed at 2.5°, and the tool down force was kept constant about 7.5 kN. The direction of the tool rotation was counter-clockwise, and the advancing and retreating sides were accordingly marked.

The rotating speed (ω) of the tool was 1500 rpm, and the traverse speed of the pin (v) was 40 mm/min. Quenching water was immediately poured on the alloy plate after FSP to prevent accumulative heating. To understand the effect of heat treatment on the microstructure of the Al-Zn-Mg-Cu-Ni alloy, both alloy A and FSP-processed alloy B were subjected to homogenization, artificial aging treatment and retrogression and re-aging (RRA) according to the steps presented in Table 2. Heat treatments are considered optimal for the Al alloys in this study as have been reported [1–3, 6]. Each step of the treatment was followed by immediate quenching with cold water as reported [2].

Alloy A (as-cast) and alloy B (FSP-processed) samples were ground and polished with 0.5 μm diamond paste at the final stage. The samples were etched using Keller's reagent to reveal the microstructure. The microstructural evaluation was performed via optical microscopy (OM, Olympus PMG3) and scanning electron microscopy (SEM) followed by coupled energy dispersive X-ray spectroscopy (EDS, JEOL JSM-6460LA) and X-ray diffraction analysis (XRD). XRD measurements were conducted using a D2 PHASER diffractometer with Cu $K\alpha$ radiation (λ = 1.54184 Å) at 30 kV and 10 mA. The XRD patterns were recorded within the 2° range of 20° to 80° with a step size of 0.02 and an effective total time of 651.2 s. The grain size was evaluated via the mean linear intercept method. The Vickers microhardness of the specimens was determined with 30 N loads and a dwell time of 10 s. Each reading was conducted for five times on the average.

3. RESULTS AND DISCUSSION

Figure 2a shows the microstructure of (Al–Zn–Mg–Cu–Ni) alloy A. The microstructure of the as-cast alloy A mainly consisted of Ni flakes that were dis-

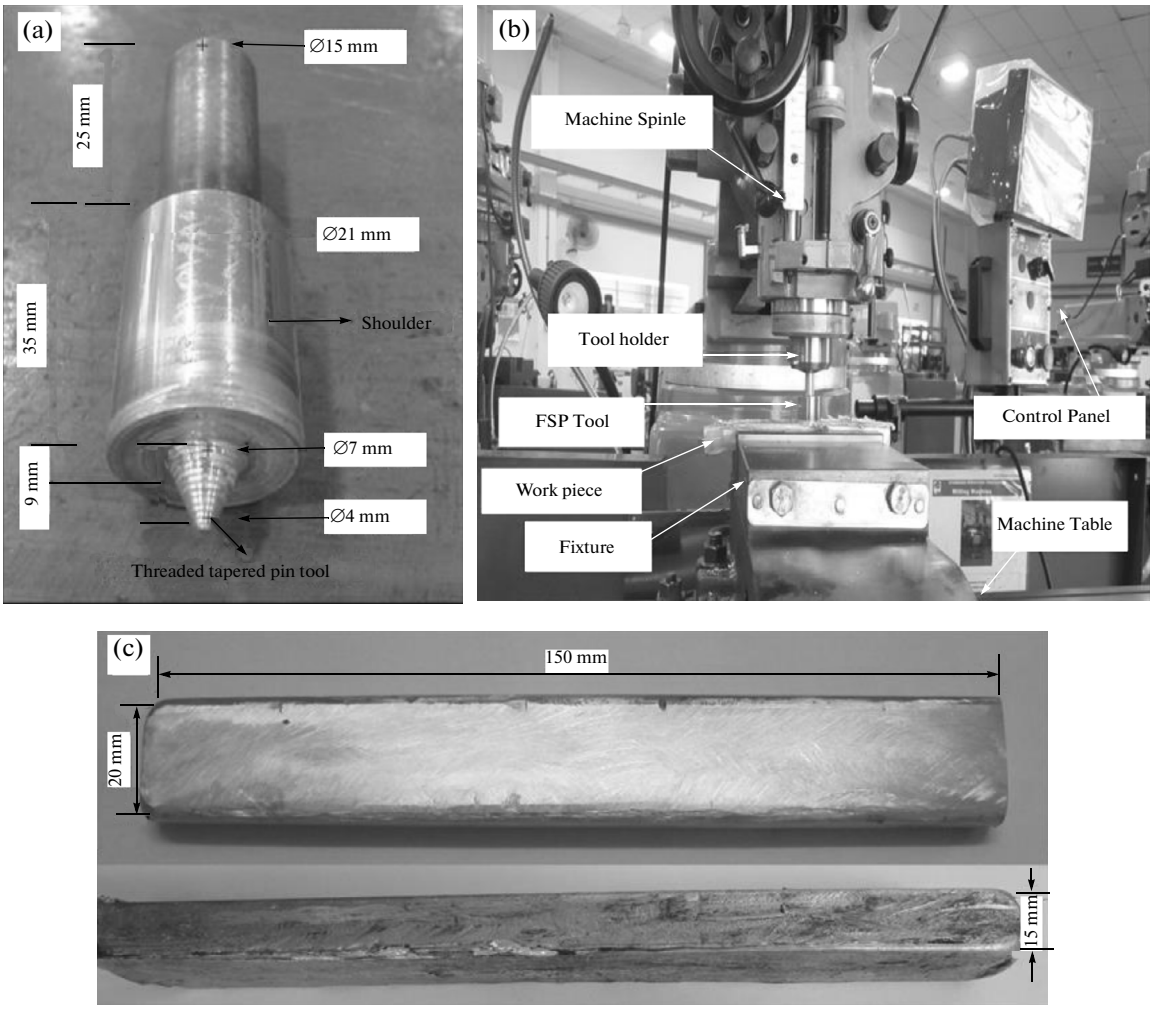

Fig. 1. Schematic illustration of (a) FSP tool, (b) FSP machine, and (c) work piece samples.

tributed along the α-Al dendrites. Figure 2a shows that the distribution of the Ni flakes in the base alloy was not homogeneous. The average grain size of as-quenched alloy was about 25.40 μm.

Figure 2b shows the SEM images of the samples' microstructures. The SEM images show that the Ni particles were irregularly distributed and were dispersed in the Al–Zn–Mg–Cu matrix and almost directly bonded without any cracks or voids between them. The EDS spectra of these regions, shown in Fig. 2c, indicate that the Ni content of the alloy was 15.34 at % which is the typical value for Al–Ni alloys, as is subsequently shown.

Figure 3a shows the OM of an Al–Zn–Mg–Cu–Ni alloy sample after homogenization and age tempering at T6. The average grain size of the alloy was about 28.3 μm. Conventionally, the volume fraction of the dendritic network structure progressively decreases and the residual phases become small and sparse because of the heat treatment effects.

The SEM images in Fig. 3b show the flake shape of the intermetallic structure of the Al–Ni alloy, which was homogeneous and had excellent interface bonding within the Al matrix. The results of the EDS scan analysis shown in Fig. 3c reveal that the Ni content decreased because it reacted with Al. Figure 4a shows the OM of alloy A after RRA. The SEM image in Fig. 4b illustrates the bright areas, which denote the newly formed phases in addition to the dispersed particles. Figure 4c shows the stoichiometric content of the Al matrix after Ni addition, as was determined via EDS.

The alloy microstructure after FSP could be classified into three major regions, namely, SZ, thermo-mechanically affected zone, and heat-affected zone [16]. Fig. 5 a shows that these regions in the FSP-processed alloy B were affected by a threaded taper pin tool. The microstructure of SZ was evidently different

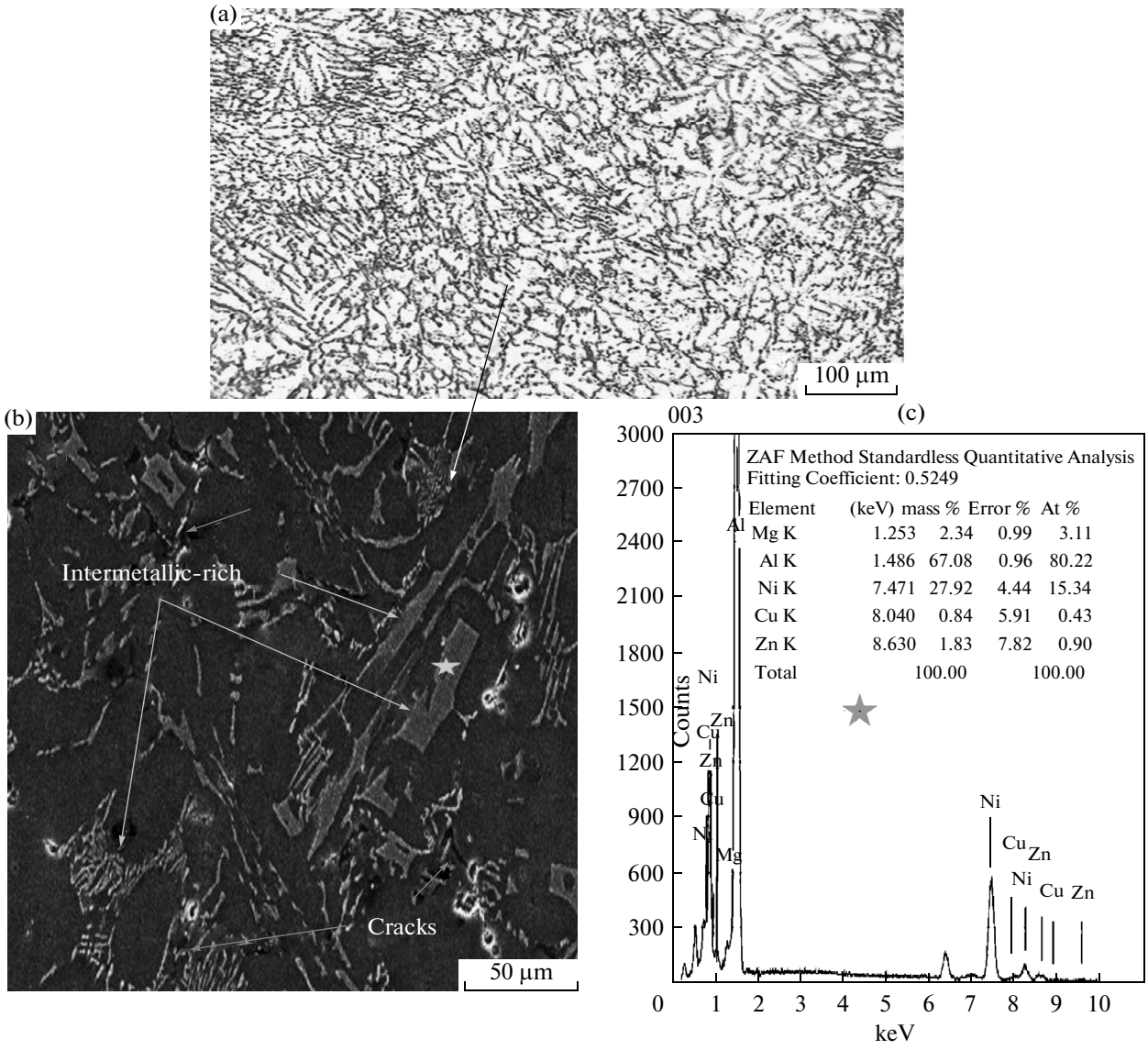

Fig. 2. (a) OM of Al-Zn-Mg-Cu-Ni alloy (as-quenched); (b) SEM of microstructure; (c) energy dispersive X-ray spectroscopy analysis.

from the base material (BM) (alloy A). The average grain size in the SZ was approximately 14.3 μm. The intense plastic deformation and frictional heating during FSP generated a recrystallized and fine-grained microstructure within SZ. This phenomenon is known as dynamic recrystallization [17–20]. The SEM micrographs of alloy B shown in Fig. 5b shows the particle distribution in the SZ. Figure 5c shows the EDS spectrum obtained for the particle-rich region, which confirmed the presence of Ni dispersoids. During FSP, a higher heat input associated with an increase in the rotational speed or decrease in traveling speed facilitates grain growth and consequently coarsens the recrystallized grains [21]. In addition, the reinforcing Ni particles could function as barriers against grain boundaries and impede grain growth by limiting their movement.

This event is known as the pinning effect [18, 22]. According to Barmouz et al. [23], a significant number of nucleating sites are produced during plastic deformation. Concurrently, during dynamic recrystallization, the nucleation of new grains at preferential sites occurs. Moreover, the reinforcement particles increase the nucleation sites for recrystallization. As the number of the primary recrystallized grains increases, the final microstructure becomes finer.

When the FSP-processed alloy B microstructure was subjected to T6 treatment, distributed equiaxed particles were obtained, as is shown in Fig. 6a. The average grain size of the FSP-processed alloy B slightly

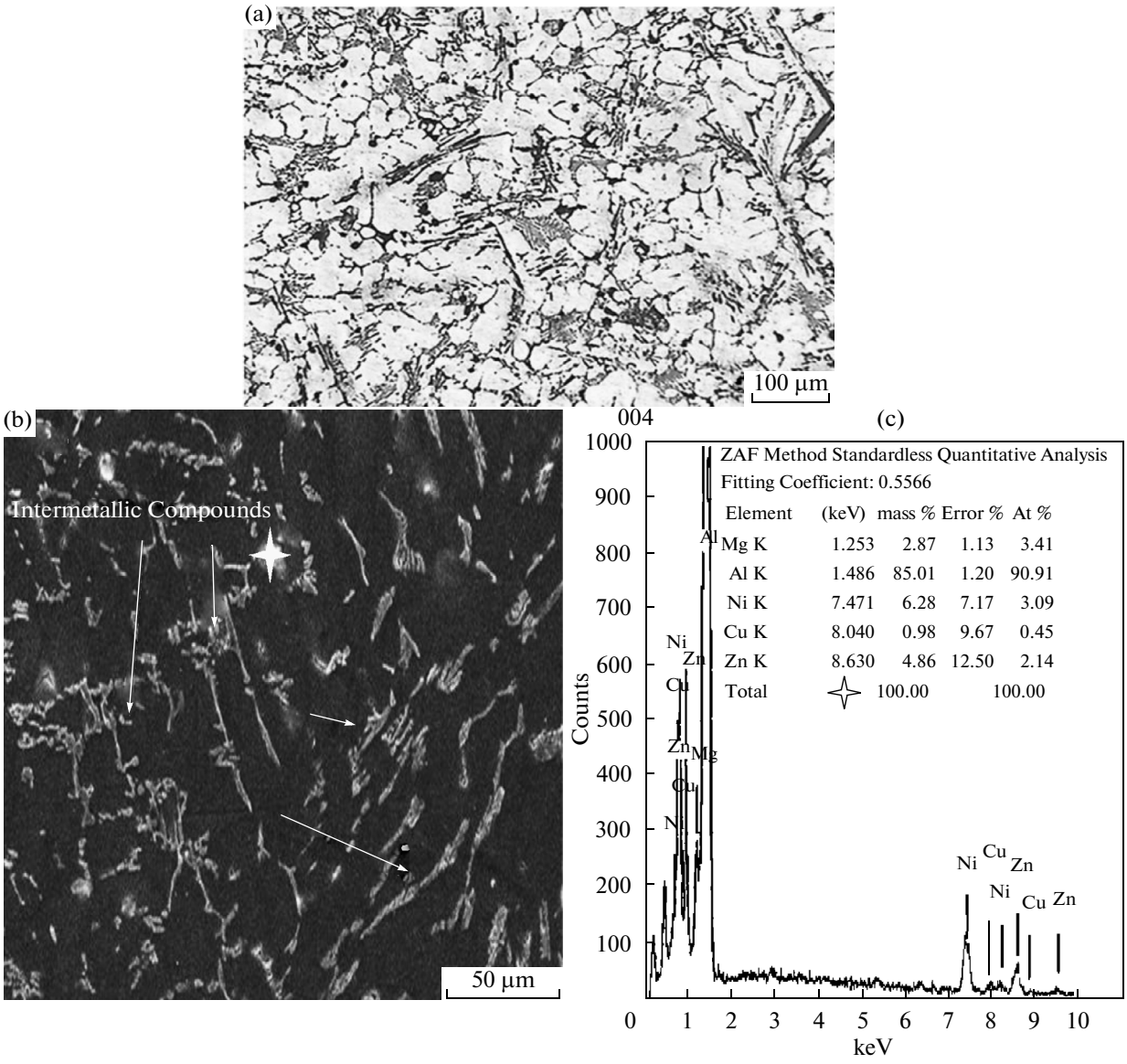

Fig. 3. (a) OM; (b) and (c) SEM micrograph and EDS scan analysis results of alloy A microstructure showing intermetallic properties after homogenization and age tempering at T6.

increased at about 16.5 μm, (for the center of the SZ) as a result of the homogenization and heat treatment [21]. The SEM micrograph shown in Fig. 6b reveals that the volume fraction of the Ni-rich particles was high in the Al matrix. The EDS microanalysis results shown in Fig. 6c proved the increasing Ni content within the matrix.

Figure 7a shows the alloy B microstructure sample analyzed after FSP and RRA. Two distinct regions were marked, including the thermo-mechanically affected zone and SZ. The heat-affected zone was not identified in the BM in the alloy B microstructure.

The microstructures of alloys A and B were compared to determine the effect of RRA. The BM microstructure of alloy A (Fig. 4a) primarily consisted of α-Al and Al–Ni eutectic structure with an average grain size of 29 μm. The alloy B microstructure (Fig. 7a) consisted of a SZ with homogeneously dispersed Ni particles in the α-Al matrix. The average grain size was about 18 μm (in the SZ) for the alloy B microstructures. Figure 7b shows that SZ had finer reinforcement particles, which were more evenly distributed throughout the matrix. This phenomenon was primarily caused by heat generated during the stirring action [24, 25].

Furthermore, at a high D/d ratio (D: shoulder diameter of 21 mm, d: pin diameter of 7 mm), excess amount of heat is generated, which resulted in a turbu-

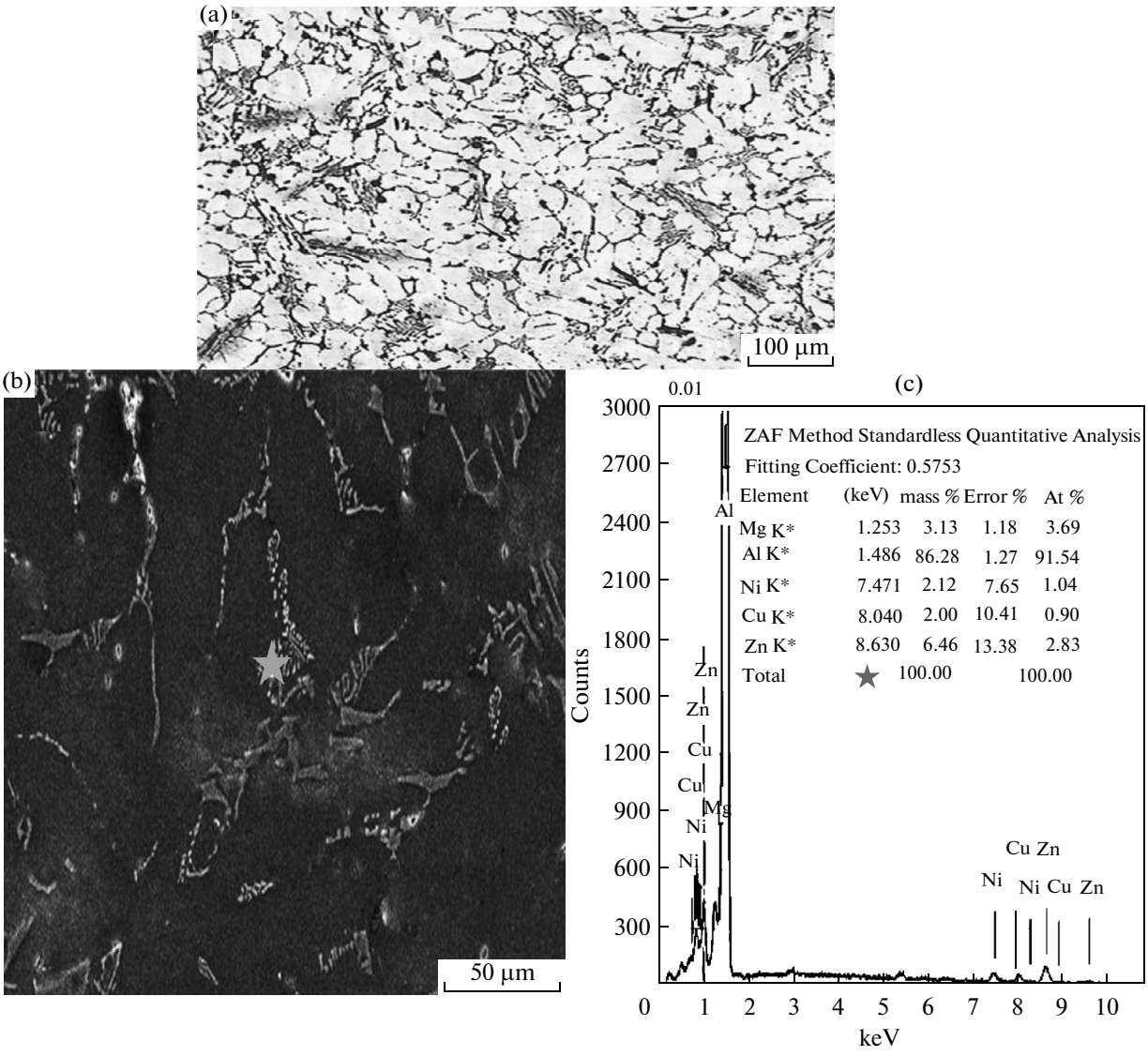

Fig. 4. (a) OM; (b) SEM image; and (c) EDS micro analysis results of alloy A microstructure after RRA.

lent type of material flow that leads to consolidation within the FSP-processed region as previously reported [26]. Fine precipitates were formed within the matrix because of the RRA effect. EDS scan analysis results shown in Fig. 7c show the Ni-rich dispersed particles in the matrix.

XRD analysis was performed to verify the presence of the intermetallic phases and phase transformation in the alloys after heat treatment. Figure 8c shows the XRD patterns of alloy A after quenching in cool water. The primary eutectic system mainly consisted of the α-Al peak in addition to the Al_4Ni_3 and $MgZn_2$ phases detected through a small peak. Figure 8b shows the XRD analysis of alloy A after age tempering at T6. The figure shows that the product was composed of α-Al and $MgZn_2$ as the major phases and a small amount of Al_7Cu_4Ni and Al_4Ni_3 as the residual phases. $MgZn_2$, as a major phase, was present because of the subsequent homogenization in the aging treatment at T6, as was previously reported [3, 6]. Figure 8a shows the XRD patterns of alloy A after RRA. The figure reveals that the principal peaks of α-Al and the Mg_2Zn_{11} originate from $MgZn_2$ and Al_4Ni_3 phases. In RRA, most of the $MgZn_2$ phase was transformed into other forms, such as Mg_2Zn_{11} [2, 3].

Figure 9c shows the XRD patterns for alloy B after FSP. The figure shows the main peaks of the Al and Al-Ni phases and a small peak for Al_3Ni_2 in addition to a minute Al_7Cu_4Ni phase. The significantly increasing reaction between the Ni-rich particles and Al matrix

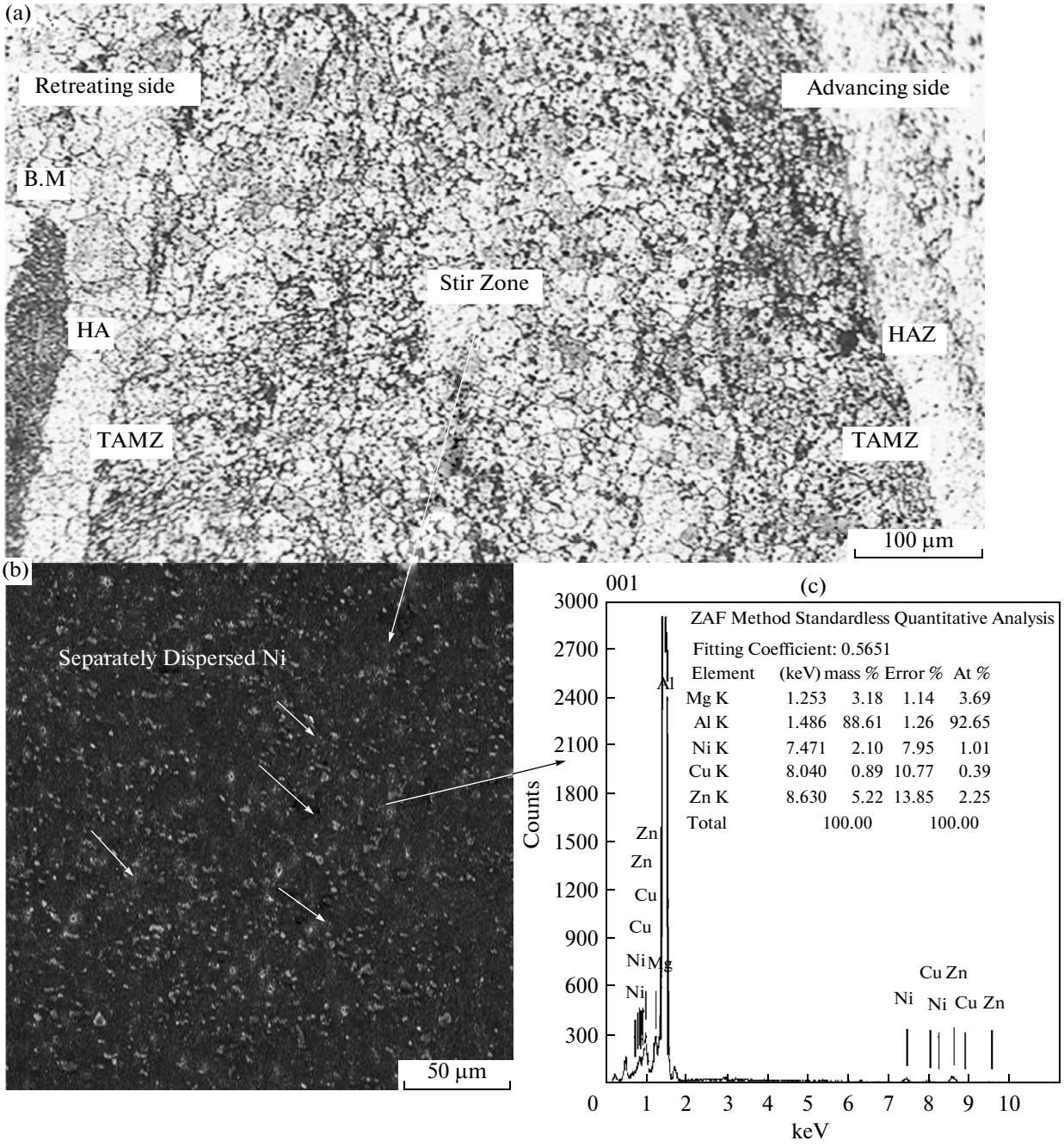

Fig. 5. (a) OM of FSP-processed (Al-Zn-Mg-Cu-Ni) alloy B presenting different regions; (FSP parameter: 1500 rpm, 40 mm/min); (b) to (c) SEM micrograph and EDS spectrum of the microstructure of dispersed particles in the stir zone (SZ).

evidently led to the appearance of numerous Al-Ni phases. This phenomenon is caused by the high temperature generated during FSP, as was previously reported [27, 28], in addition to a high D/d ratio of the FSP tool in this study. The temperature of the SZ ranged from 400°C to 500°C during the FSP of the Al-Zn–Mg–Cu alloy [29]. Figure 9b shows the XRD patterns of alloy B after age tempering at T6, which reveals the presence of α-Al, Al–Ni, and Al_3Ni_2 as the main phases. Figure 9a shows the XRD patterns of alloy B after RRA. The figure shows that the major phases were Al and Al-Ni, in addition to the numerous Al_7Cu_4Ni, Al_4Ni_3, $MgZn_2$, and Mg_2Zn_{11} phases. In summary, several intermetallic phases of Al-Ni were generated within a range of temperature, based on the Al-Ni phase diagram [30].

The quenched alloy A samples were alloys A-T6 and A-RRA. The Vickers hardness values were deter-

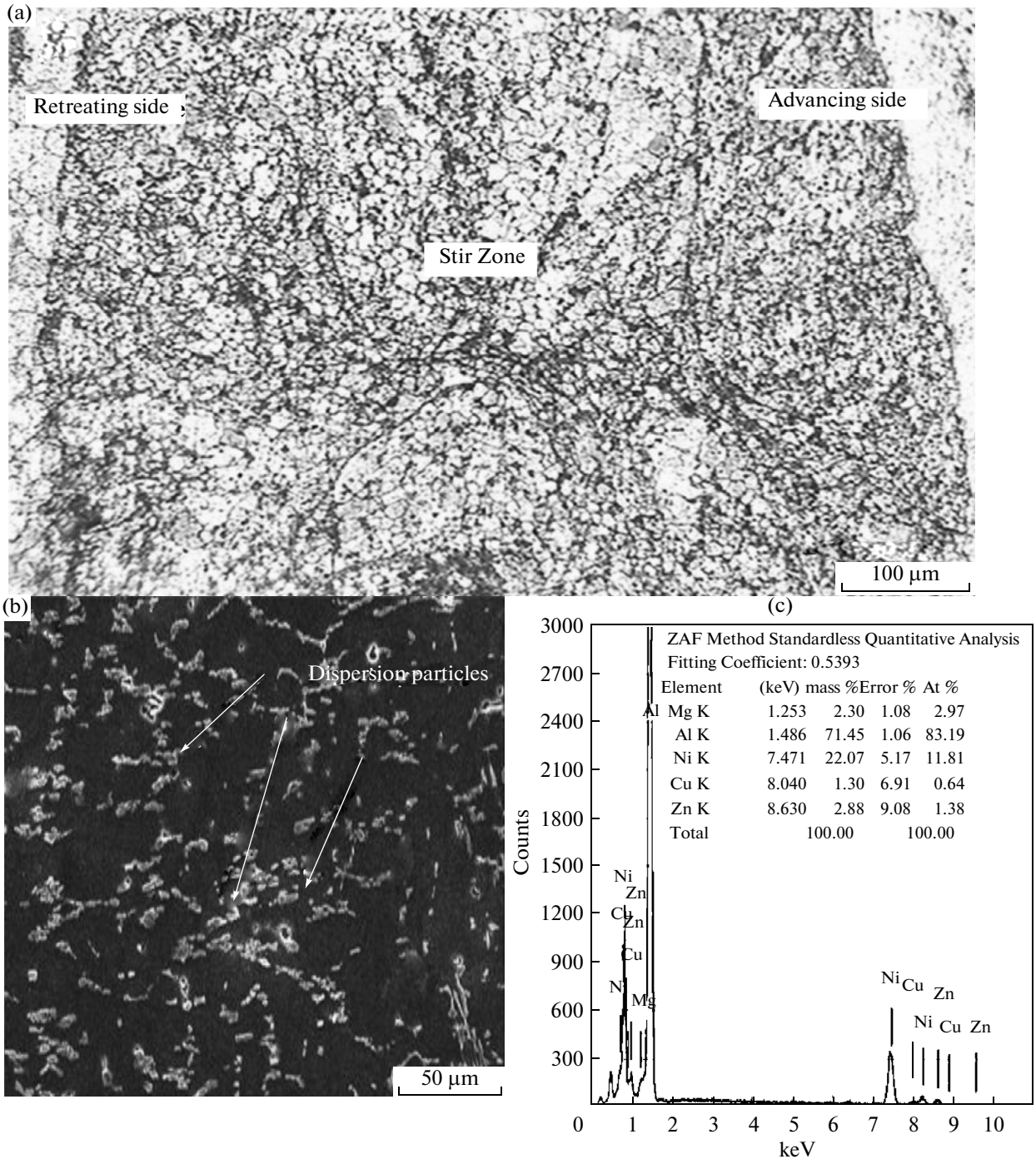

Fig. 6. (a) OM; (b) SEM micrograph; and (c) EDS scan analysis results of FSP-processed alloy B microstructure (at SZ) after age tempering at T6.

mined for as-quenched alloy A to be 135 *HV*. The results show that the hardness value significantly increases after applying a series of heat treatments to achieve 200 and 208 *HV* values for the alloy after age tempering at T6 and RRA, respectively. This result can be attributed to the precipitation hardening of the alloy element, as was previously reported [1, 2]. In addition, the interfacial bonding between the Al matrix and Ni compounds was substantial (Figs. 3 and 4b). By contrast, the dislocation by-passing of the dispersed particles of the Ni compounds was based on the Orowan mechanism, which was also

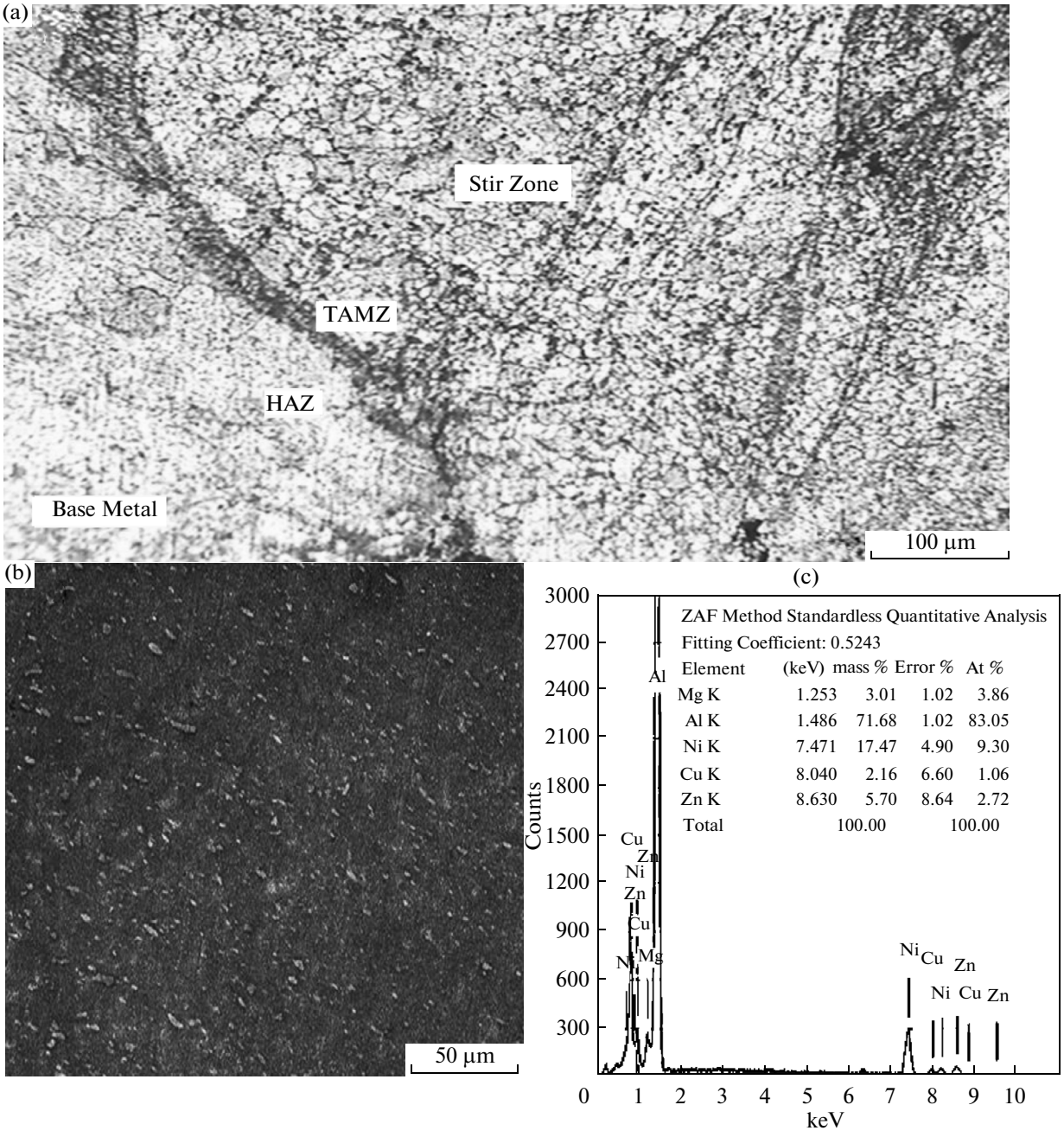

Fig. 7. (a) OM of FSP-processed alloy B showing parent metal and regions of FSP; (b) SEM and (c) EDS spectrum of FSP-processed alloy microstructure at SZ after RRA.

responsible for the increased strength, as was previously reported [31]. After FSP, age tempering at T6 and RRA heat treatments on the Al–Zn–Mg–Cu–Ni (alloy A) alloy, maximum gains of about 50, 45, and 54 *HV*, respectively, were achieved for the Vickers hardness of all alloy B samples in the center of SZ. This enhancement may be explained by several reasons. First, the material flows that were imposed during FSP promote grain redistribution because of the presence of the threaded taper pin tool structure. This action increased the plastic deformation in the Al matrix through substantial grain refinement. According to the Hall-Petch relationship [32], $H = H_0 + k_H d^{-1/2}$, where H is the final hardness, H_0 and k_H are constants, and d is the grain size, a decrease in the grain size increases the hardness. Second, a high density of the dislocations pinned by the fine dispersed Ni particles was observed (Fig. 5b). In addi-

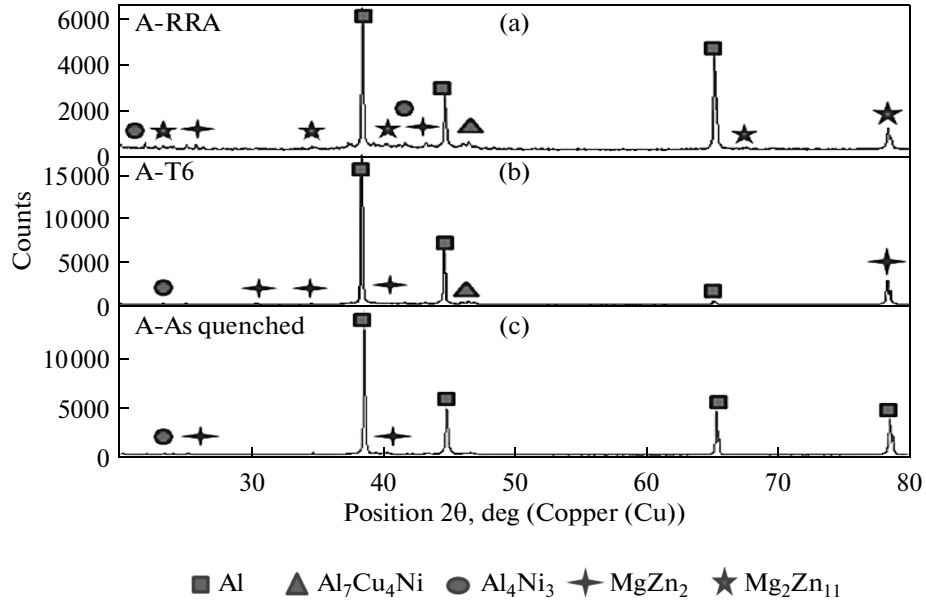

Fig. 8. XRD plots for alloy A after quenching, T6 tempering, and applying RRA.

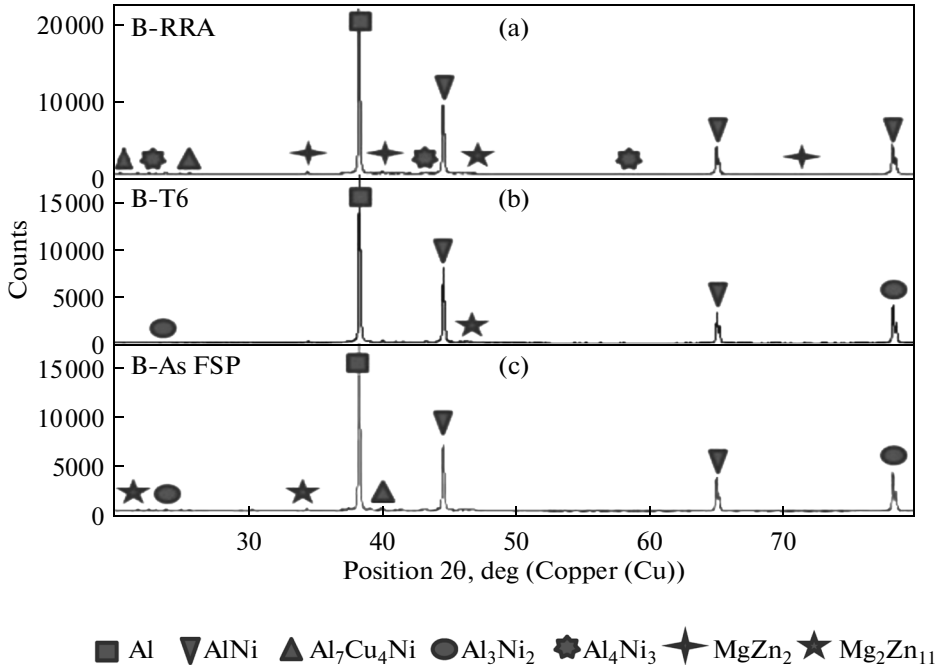

Fig. 9. XRD patterns for alloy B after FSP, age tempering at T6, and RRA.

tion, at a high tool rotation rate (1500 rpm), more precipitates dissolved into the Al matrix because of the high temperature, which would re-precipitate as fine particles in FSP. Furthermore, the alloy B samples that were age-tempered at T6 and underwent RRA were harder compared with the FSP-processed sample. This phenomenon was caused by the additional precipitation hardening of the alloy samples.

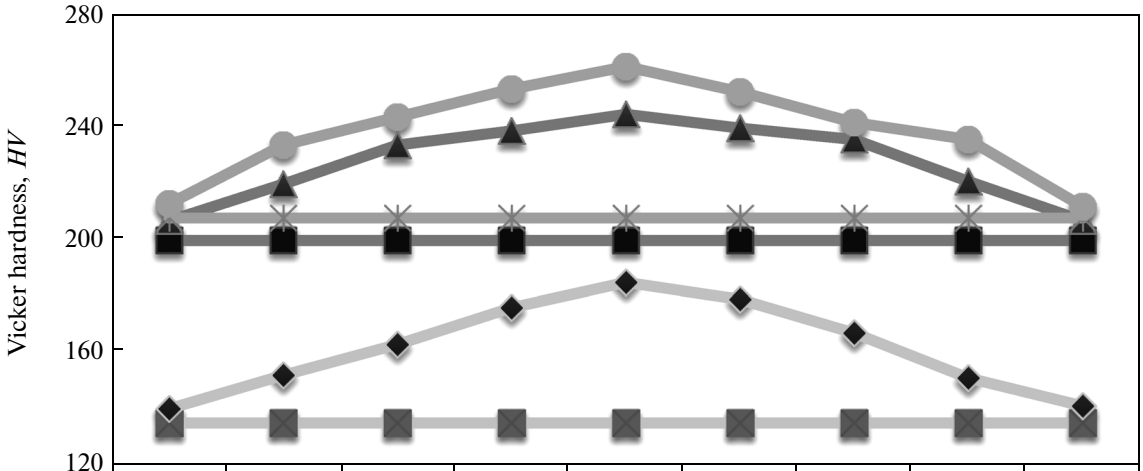

	–8	–6	–4	–2	0	2	4	6	8
As quenched	135	135	135	135	135	135	135	135	135
As FSPed	140	152	163	176	185	179	167	151	141
Alloy A-T6	200	200	200	200	200	200	200	200	200
Alloy B-T6	207	220	234	239	245	240	236	221	207
Alloy A-RRA	208	208	208	208	208	208	208	208	208
Alloy B-RRA	213	234	244	254	262	253	242	236	212

Distance from center of stir zone, mm

Fig. 10. Comparison of the Vickers hardness values of alloys A and B after FSP and heat treatment.

4. CONCLUSIONS

(1) Microstructural analysis of the Al–Zn–Mg–Cu alloys with Ni particles had revealed coarse dispersed Ni particles with an average grain size of approximately 25.40 μm. The evaluation of the Al–Zn–Mg–Cu–Ni alloy microstructure after FSP with a threaded tapered pin tool reveals that the SZ consisted of fine, homogeneous, and dispersed Ni particles, which had excellent interfacial bonding with the Al matrix. The grain size was about 18 μm (in the SZ).

(2) The XRD patterns of the Al–Zn–Mg–Cu–Ni alloy before FSP show that the α-Al and $MgZn_2$ were the major phases and that residual Al_7Cu_4Ni and Al_4Ni_3 phases were present in the alloy matrix after a series of heat treatments. After FSP, the evaluations of the alloy B microstructure show that α-Al, Al-Ni, and Al_3Ni_2 were the main phases because of the high temperature generated with stirring and the shape of the FSP tool. Moreover, numerous Al_7Cu_4Ni, Al_4Ni_3, $MgZn_2$, and Mg_2Zn_{11} phases were formed after a series of heat treatments.

(3) The Vickers hardness value for alloy A increased after age tempering at T6 and RRA due to the precipitation and dispersion strengthening. Alloy B (after FSP) became harder than alloy A because of the stirring action of the FSP tool, grain refinement, additional precipitates, and dispersed Ni particles.

ACKNOWLEDGMENTS

This work is supported under the University Malaysia Perlis (UniMAP). The authors gratefully acknowledge the outstanding support provided by the technicians of the work shop of Materials Engineering School, UniMAP.

REFERENCES

1. H. T. Naeem, K. S. Mohammed, K. R. Ahmed, and A. Rahmat, "A comparative study of additives of nickel, cobalt, tin affecting the microstructures and mechanical properties of Al–Zn–Mg–Cu alloys," Pensee J., **76** (3), 218–235 (2014).
2. H. T. Naeem, K. R. Ahmad, K. S. Mohammad, and A. Rahmat, "Evolution of the retrogression and reaging treatment on microstructure and properties of aluminum alloy (Al–Zn–Mg–Cu)," Adv. Mater. Res. **925**, 258–262 (2014).
3. H. T. Naeem, K. S. Mohammad, K. R. Ahmad, and A. Rahmat, "The influence of nickel and tin additives on the microstructural and mechanical properties of Al–Zn–Mg–Cu alloys," Adv. Mater. Sci. Eng., **2014**, Art. ID 688474 (2014).

4. P. Cavaliere, "Effect of friction stir processing on the fatigue properties of a Zr-modified 2014 aluminium alloy," Mater. Charact., **57**, 100–104, (2006).
5. Y. Gao, Y. Zhang, and X. Liu, "Influence of trace Ti on the microstructure, age hardening behavior, and mechanical properties of an Al–Zn–Mg–Cu–Zr alloy," Mater. Sci. Eng., A **598**, 293–298 (2014).
6. H. T. Naeem, K. S. Mohammad, and K. R. Ahmad, "The effect of microalloying of nickel and RRA treatment on microstructure and mechanical properties for high strength aluminum alloy," Adv. Mater. Res. **925**, 253–257 (2014) .
7. I. Nikulin, R. Kaibyshev, and T. Sakai, "Superplasticity in a 7055 aluminum alloy processed by ECAE and subsequent isothermal rolling," Mater. Sci. Eng., A **407**, 62–70 (2005).
8. M. R. Rezaei, M. R. Toroghinejad, and F. Ashrafizadeh, "Effects of ARB and ageing processes on mechanical properties and microstructure of 6061 aluminum alloy," J. Mater. Process. Technol. **211**, 1184–190 (2011).
9. A. Rao. B. Rao, V. Deshmukh, A. Shah, and B. Kashyap, "Microstructural refinement of a cast hypereutectic Al–30Si alloy by friction stir processing," Mater. Lett. **63**, 2628–2630 (2009).
10. Z. Ma, "Friction stir processing technology: A review," Metall. Mater. Trans. A **39**, 642–658 (2008).
11. R. S. Mishra and Z. Y. Ma, "Friction stir welding and processing," Mater. Sci. Eng.: R: Reports **50**, 1–78 (2005)
12. T. Dieguez, A. Burgueño, and H. Svoboda, "Superplasticity of a friction stir processed 7075–T651 aluminum alloy," Proc. Mater. Sci. **1**, 110–117 (2012).
13. A. Orozco-Caballero, C. Cepeda-Jiménez, P. Hidalgo-Manrique, P. Rey, D. Gesto, D. Verdera, et al., ""Lowering the temperature for high strain rate superplasticity in an Al–Mg–Zn–Cu alloy via cooled friction stir processing," Mater. Chem. Phys. **142**, 182–185 (2013).
14. M. El. R. Magdy, E. A. El. Danaf, and M. S. Soliman, "High-temperature deformation and enhanced ductility of friction stir processed 7010 aluminum alloy," Mater. Design **32**, 1916–1922 (2011).
15. C. M. Hu, C. M. Lai., P. W. Kao, N. J. Ho, and J. C. Huang, "Quantitative measurements of small scaled grain sliding in ultra-fine grained Al–Zn alloys produced by friction stir processing," Mater. Character. **61**, 1043–1053 (2010).
16. N. M. S. Gopalakrishnan, "Prediction of tensile strength of friction stir welded aluminium matrix TiCp particulate reinforced composite," Mater. Design **32**, 462–467 (2011).
17. J.-Q. Su, T. W. Nelson, and C. J. Sterling, "Microstructure evolution during FSW/FSP of high strength aluminum alloys," Mater. Sci. Eng.: A **405**, 277–286 (2005).
18. M. El. R. Magdy and E. A. El-Danafa, "The influence of multi-pass friction stir processing on the microstructural and mechanical properties of aluminum alloy 6082," J. Mater. Proc. Technol. **212**, 1157–1168 (2012).
19. H. F. Y. Morisada, T. Nagaoka, and M. Fukusumi, "MWCNTs/AZ31 surface composites fabricated by friction stir processing," Mater. Sci. Eng.: A **419**, 344–348 (2006).
20. Q. Z. W. Blum, R. Merkel, and H. J. McQueen, "Geometric dynamic recrystallization in hot torsion of Al–5Mg–0.6Mn (AA5083)," Mater. Sci. Eng.: A **205**, 23–30, (1996).
21. M. Abbasi Ghaaracheh, A. H. Kokabi, G. H. Daneshi, B. Shalchi, and R. Sarrafi, "The influence of the ratio of "rotational speed/traverse speed"(ω/v) on mechanical properties of AZ31 friction stir welds," Int. J. Machine Tools Manufact. **46**, 1983–1987 (2006).
22. Z. Y. Maa, S. R. Sharma, and R. S. Mishra, "Effect of friction stir processing on the microstructure of cast A356 aluminum," Mater. Sci. Eng.: A **433**, 269–278 (2006).
23. M. Barmouz, P. Asadia, M. K. B. Givi, and M. Taherishargh, "Investigation of mechanical properties of Cu/SiC composite fabricated by FSP: Effect of SiC particles' size and volume fraction," Mater. Sci. Eng.: A **528**, 1740–1749 (2011).
24. Y. Morisada, H. Fujii, T. Nagaoka, K. Nogi, and M. Fukusumi, "Fullerene/A5083 composites fabricated by material flow during friction stir processing," Composites Part A: Appl. Sci. Manufact., **38**, 2097–2101 (2007).
25. S. A. Alidokht, A. Abdollah-Zadeh, S. Soleymani, T. Saeid, and H. Assadi, "Evaluation of microstructure and wear behavior of friction stir processed cast aluminum alloy," Mater. Charact. **63**, 90–97 (2012).
26. S. Cartigueyen and K. Mahadevan, "Study of friction stir processed zone under different tool pin profiles in pure copper," IOSR J. Mech. Civil Eng. **11**, Issue 2, Ver. VII, 6–12 (2014).
27. Devinder Yadav and Ranjit Bauri, "Processing, microstructure and mechanical properties of nickel particles embedded aluminium matrix composite," Mater. Sci. Eng.: A **528**, 1326–1333 (2011).
28. Jinwen Qian, Jinglong Li, Jiangtao Xiong, Fusheng Zhang, and Xin Lin, "In situ synthesizing Al_3Ni for fabrication of intermetallic-reinforced aluminum alloy composites by friction stir processing," Mater. Sci. Eng.: A **550**, 279–285 (2012).
29. C. G. Rhodes, M. W. Mahoney, W. H. Bingel, R. A. Spurling, and C. C. Bampton, "Effects of friction stir welding on microstructure of 7075 aluminum," Scr. Mater. **36**, 69–75 (1996).
30. H. Okamoto, "Al–Ni (Aluminum–Nickel)," J. Phase Euilibria, **14**, 257–259 (1993).
31. H. T. Naeem and K. S. Mohammed, "Microstructural evaluation and mechanical properties of an Al–Zn–Mg–Cu-alloy after addition of nickel under RRA conditions," Mater. Sci. Appl. **4**, 704–711 (2013).
32. X. Feng, H. Liu, and S. S. Babu, "Effect of grain size refinement and precipitation reactions on strengthening in friction stir processed Al–Cu alloys," Scr. Mater. **65** 1057–1060 (2011).